Ibn Al-Haitham Journal for Pure and Applied Sciences
Journal homepage: jih.uobaghdad.edu.iq
PISSN: 1609-4042, EISSN: 2521-3407
IHJPAS. 2026; 39(3)

Biological Corrosion and the Application of Chelate Ligands Along with Their Metallic Complexes: A Practical and Spectra Investigation

Bushra Mohan Abdul Amir[1*] and Naser Dheyaa Shaalan[2]
[1,2] Department of Chemistry, College of Sciences for Women, University of Baghdad, Baghdad, Iraq
[*]Corresponding Author

Received: 19/January/2026
Accepted: 14/April/2026
Published: 20/July/2026
doi.org/10.30526/39.3.4422

Abstract
The Schiff base (E)-N'-(furan-2-ylmethylene)-2-hydroxybenzohydrazide tridentate was synthesized using conventional condensation techniques, and a series of metal compounds were prepared using its chlorides, including Mn^{+2}, Co^{+2}, Ni^{+2}, Cu^{+2}, Zn^{+2}, and Zr^{+4}. The synthesized compounds were subjected to FTIR, UV-Vis, ESI-MS, NMR, CHN, and TGA, as well as their derivatives (DTG). The physical properties of the synthesized compounds, including their magnetic susceptibility, conductivity, and ion detection capabilities, were investigated. Corrosive bacteria were isolated from oil-associated water at the Al-Durra refinery site, along with two types of fungi and yeasts. The activity of these compounds against the corrosive isolates and four pathogenic strains was evaluated at a concentration of 10^{-3} mol/L. The fungi exhibited resistance to the synthesized compounds, and the results showed that these compounds were more effective against pathogenic strains than against the isolates, demonstrating the isolates' high adaptability to harsh organic environments. An on-site chlorine solution was used as a control. The results for the newly synthesized Schiff base (L2) and its compounds showed high efficacy compared to the on-site chlorine solution, demonstrating the success of the structural design and indicating their suitability as additives for corrosion-resistant coatings or future pharmaceuticals.
Keywords: *Absidia carmbivira* fungus, *Bacillus* bacteria, Corrosion zones, Microbiological corrosion, *Portris acaladia* fungus, Schiff base

1. Introduction

Microbial corrosion is one of the most complex forms of corrosion, arising from a combination of electrochemical processes and the metabolic activity of microorganisms, particularly sulfate- and nitrate-reducing bacteria. These organisms accelerate metal corrosion by forming biofilms and altering the chemical properties of the environment surrounding the metal surface, such as pH, oxygen concentration, and charge distribution[1]. This leads to the deterioration and damage of structures, tools, and equipment made of iron and other corrosive metals, including oil, water, and sewage pipelines, as well as other industrial facilities[2]. In 2016, experts from the National Association of Corrosion Engineers (NACE International) estimated the total global cost of corrosion at approximately US$2.5 trillion, accounting for significant environmental, health, and safety consequences[3]. The causes of anaerobic corrosion, especially in iron, remained unknown and puzzled researchers until the late 19th century, when Garrett (1891) made early observations linking bacterial activity to corrosion of metals in soil. However, the scientific foundations of microbial corrosion were laid in 1934 by von Olzogen-Kohr and van der Vlugt through their theory of cathodic depolarization, which explained the accelerated corrosion of iron by sulfate-reducing bacteria. The activity of these microorganisms leads to the formation of iron sulfide, a reliable indicator of their presence under these conditions. At the same time, no other microbial group exhibits similar detrimental effects when cultured under

controlled conditions. Various methods have been explored to combat corrosion[4], including antioxidant coatings[5]. Furthermore, there has been interest in using natural and environmentally friendly materials, such as wood glue, as corrosion inhibitors[6]. In addition, treatments using corrosion-resistant materials such as AISI 304 and AISI 316 carbon steel alloys, fiberglass, or epoxy have been employed to address this problem[7]. Despite these treatments, which have imposed high economic costs and, in some cases, succeeded in reducing or mitigating corrosion, research continues to identify more economical and comprehensive solutions[8]. Some researchers have explored biological approaches to addressing this phenomenon by introducing specific fungi that feed on anaerobic bacteria. Therefore, a previous study isolated all organisms present at the selected research site and evaluated the effectiveness of the prepared compounds against them, and determined whether these fungi support or inhibit the presence and reproduction of harmful bacteria, or have no effect[9]. Organic compounds containing electron-donating atoms, such as nitrogen, oxygen, and sulfur, have received considerable attention for their effectiveness as corrosion inhibitors. Hydrates are among the most promising classes in this field[10], due to their high adsorption capacity on metal surfaces through coordinate bonding and electrostatic interactions. Moreover, they play a dual role in biological corrosion systems. First, these compounds act as electrochemical inhibitors by forming an adsorbed protective layer that reduces the rate of metal oxidation and reduction. Secondly, these compounds act as potential biological inhibitors by hindering microbial adhesion and preventing biofilm formation[11]. Furthermore, the presence of π-bonds and unpaired electron pairs on nitrogen and oxygen atoms enhances the interaction of these compounds with the metal surface, thereby reducing charge transfer at the metal-solution contact point[12]. This study aims to prepare and characterize compounds that effectively protect iron from biological corrosion by inhibiting the microbes that cause it.

2. Materials and Methods

All materials used are from Merck Trading Company, the Sigma-Aldrich brand. Fourier transform infrared (FTIR) spectra were recorded in the 4000–4000 cm^{-1} frequency range using a Shimadzu 8400 spectrometer, while potassium bromide (KBr) and cesium iodide spectra were recorded in the 200–4000 cm^{-1} frequency range for the compounds at room temperature. The analysis was performed in the Science Laboratory at the University of Baghdad. Ultraviolet and visible spectra were recorded using a Shimadzu UV-1800 spectrometer with two identical 10 mm quartz cells. The electronic transitions of the compounds were measured at the Services Laboratory of the College of Science for Women, University of Baghdad. The masses of the ligands and their compounds were determined using electrospray ionization mass spectrometry (ESI-mass) with a Shimadzu LCMS 2010 and nuclear magnetic resonance (^{1}H, ^{13}C NMR) spectroscopy with a Birker spectrometer at 300 MHz. Weight loss was also monitored using thermogravimetric analysis (TGA) and its derivatives (DTG). All these analyses were performed in the laboratories of Shahid Beheshti University in Tehran, Iran.

2.1. Preparation of Schiff base L_2 ligand

In a 50 mL flat-bottomed flask, equal amounts of furfural (1 mmol, 0.126 g) and 2-hydroxybenzohydrazide (1 mmol, 0.2 g) were condensed in 15 mL of pure ethanol at 40–50 °C. A drop of glacial acetic acid was added to the furfural before the amine was added to form a carbon cation. The mixture was left to stand for 5 hours, during which a yellowish-white (beige) precipitate formed. The mixture was filtered, washed with cold alcohol, and dried at 80 °C. The melting point was measured and found to be between 243 and 245 °C[13].

2.2. Preparation of metal Schiff base L_2 complexes

In a flat-bottom flask, 0.15 g (2 mmol) of a Schiff base was dissolved in 10 mL of a 50:50 mixture of pure ethanol and methanol. To ensure complete dissolution, a few drops of dimethylformamide (DMF) were added, followed by the equivalent weight (1 mmol) of a divalent metal salt chloride dissolved in 10 mL of pure ethanol (Mn^{+2}, Co^{+2}, Ni^{+2}, Cu^{+2}, Zn^{+2}) or

metal salts with higher oxidation states (Zr^{+4}). The reaction mixture was stirred at 40–50 °C for 7 hours until the solution changed color and a precipitate formed. The solution was filtered, the precipitate dried, washed with distilled water, and then purified with dry ether. The melting points were then measured[14]. The pathway of synthesis of metal complexes from Schiff bases is illustrated in **Scheme 1**.

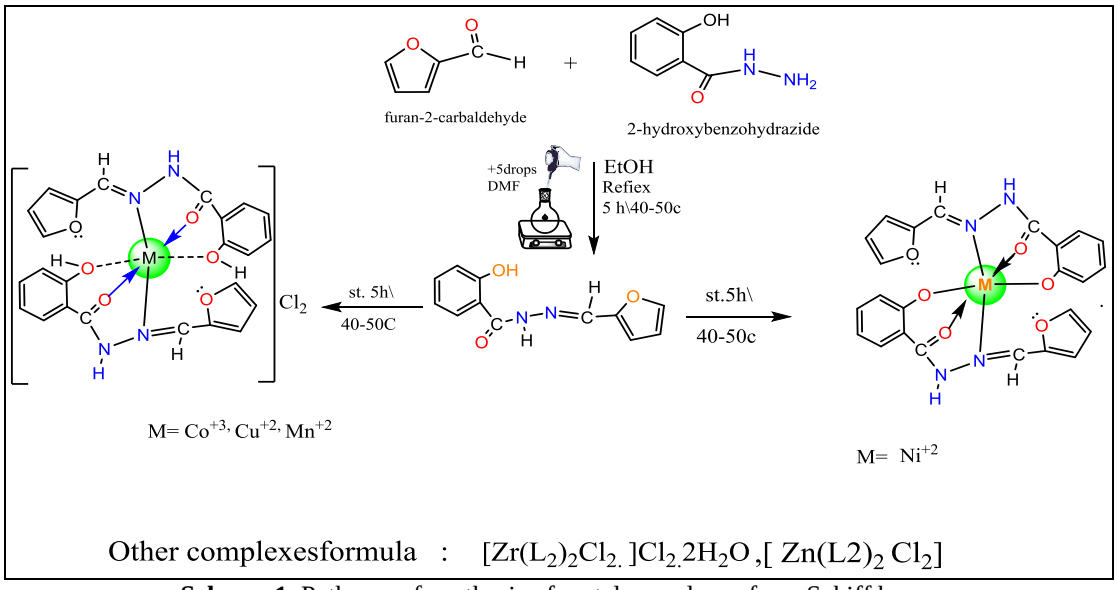

Scheme 1. Pathway of synthesis of metal complexes from Schiff bases

3. Results

3.1. Physical and analytical data

Some physical properties and analytical data of the prepared compounds are shown in **Table 1**.

Table 1. Physical data and some analytical data for the synthesized ligand (L_2) and its complexes

Formula suggestion	Color	M.P (C°)	Yield (%)	MWt g.mol^{-1}	Elemental analysis found (Calc) %			
					C	H	N	M
$C_{12}H_{10}N_2O_3$	Creamy white	245	80	230.2	63.60 (62.61)	4.11 (4.38)	13.17 (12.17)	-------
$C_{24}H_{20}N_4O_6\ MnCl_2$ $[Mn(L2)_2]Cl_2$	Light pink	265d	76	586	49.17	3.44	9.56	9.37
$C_{24}H_{20}N_4O_6CoCl$ $[Co(L2)_2]Cl_2$	Pink	287d	95	626	46.07	3.22	8.95	9.42
$C_{24}H_{20}N_4NiO_6$ $[Ni(L2)_2]$	Brown	292d	78	517	55.53	3.88	10.79	11.31
$C_{24}H_{20}N_4O_6Cl_2Cu$ $[Cu(L2)_2]Cl_2$	Yellow green	297d	73	595	48.46	3.39	9.42	10.68
$C_{24}H_{19}N_4O_6Zn$ $[Zn(L2)_2Cl_2]$	Off white	219d	67	526	54.34 (54.82)	3.45 (3.83)	10.35 (10.66)	(12.43)
$C_{24}H_{27}N_4O_{10}Zr\ Cl_3$ $[Zr(L2)_2ClOH]Cl_2.3H_2O$	Yellow	>300	88	694	39.31 (39.52)	3.45 (3.32)	8.00 (7.68)	(12.51)

3.2. Infrared spectroscopy

The FTIR spectrum of the (L_2) bond extensions and their metal complexes is shown in **Table 2**.

Table 2. The FTIR spectrum of the (L_2) bond extensions and their metal complexes

Compound code	ν C=O	ν C=N	ν N-H Bending	ν N-H Stretch	ν C=C	ν C-O	ν M-N	ν M-O	ν Other bands
L_2	1662.6	1602.55	1494.83	3270	1488	1390	-	-	νOH=3750
$[Mn(L_2)_2]Cl_2$	1616.24	1573.81	1554.52	3236.33	1523.66	1390.58	422.3	526.53 588.25	νOH=31224 .47
$[Co(L_2)_2]Cl_2$	1614.31	1599.95	1558.38	3222.83	1523.66 1490.8	1390.58	487.96 435.88	563.18 590.18	νOH=3396. 41, 3375.20
$[Ni(L_2)_2]$	1610.5	1566.56	1489.0	3211.48	1480	1390	460 455	590.22 526.57	νCHAr=311 5, 3037
$[Cu(L_2)_2]Cl_2$	1641.4	1597.06	1552.7	3140.11	1489.05	1385.6	455.17	524.54 582.50	νOH=3745. 76, 3651.25νC-HAr
$[Zn(L_2)Cl_2]$	161 8.17	1575.73 1556.43	1521.73	3226.69	1488.94	1390.58	420.45 439.74	526.53 590.18	νCHAr=312 0, 3095
$[Zr(L_2)_2ClOH]Cl_2.3H_2O$	1629.7 1608.5	1556.4	1535.73	3209.33, 3257.55	1492.8 1463.8	1393.44,	439.74	522.67 584.39	νOH=3365. 55, 3395.41, 3365.5

3.3. Mass spectrometry

The ESI- mass spectrums of Schiff base ligands are shown in **Figures 1-3**.

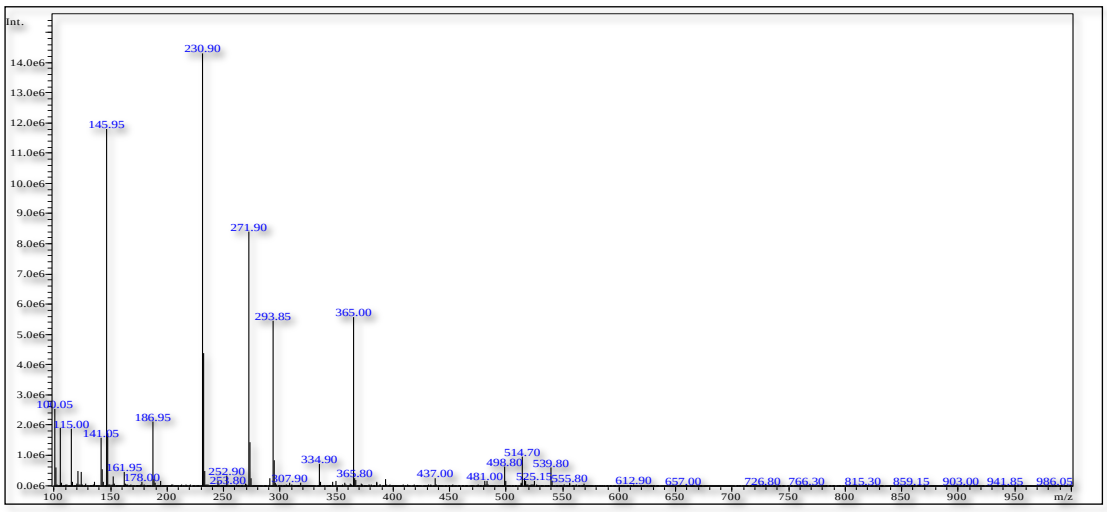

Figure 1. ESI-mass spectrum of Schiff base ligand (L_2)

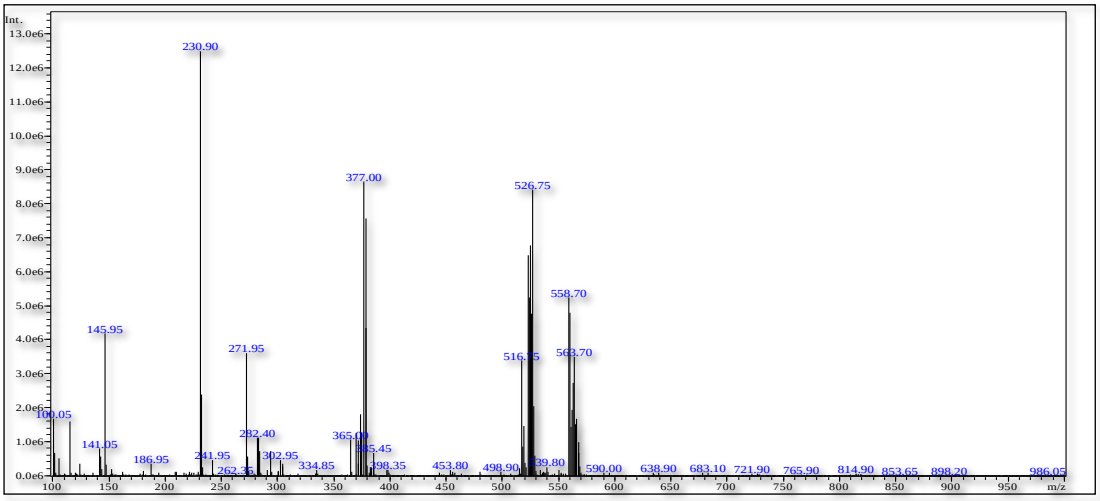

Figure 2. ESI-mass spectrum of $[Zn\ (L_2)_2Cl_2]$

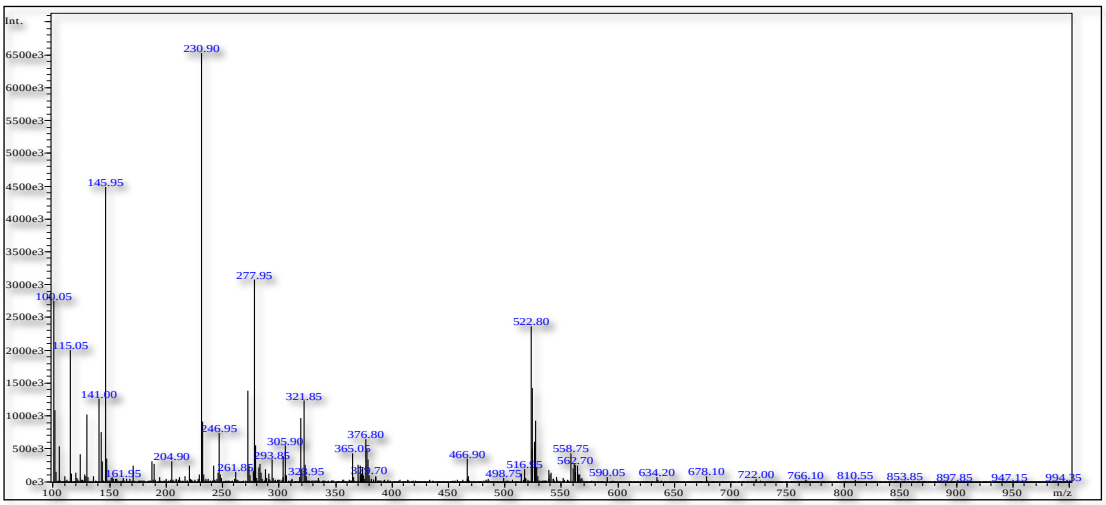

Figure 3. ESI-mass spectrum of $[Zr(L_2)_2ClOH]Cl_2$

3.4. Electronic spectroscopy

The electronic transitions of complexes CoL_2,NiL_2, CuL_2 are illustrated in **Table 3.**

Table 3. Electronic spectra, conductance in DMF solvent and magnetic moment (B.M) for ligands and their metal complexes

Compound Code	**$\Lambda_{M(DMF)}$**	**μeff B.M**	**Max (nm)**	**ν (cm^{-1})**	**Assignment**
L_2	-	-	358, 276, 238	27932.96, 36231.88, 42.16.8	π→π*, n→π*, n→π*
$[Mn(L_2)_2]Cl_2$	155	3.379	407, 363 340, 305	24570, 2548.2, 29411.76, 32786.88	$^6A_1g \rightarrow {}^4T_1g$, $^6A_1g \rightarrow {}^4T_2g$ π→π*, π→π* Aromatic
$[Co(L_2)_2]Cl_2$	137	Dia	674 608, 361	14836.79 16447.36	$A_1g_{(F)} \rightarrow T_1g$ $A_1g_{(F)} \rightarrow T_2g$
$[Ni(L_2)_2]$	38	2.8	990, 770 650	10101.01, 12987.01 15384.61	$^3A_1g_{(F)} \rightarrow {}^3T_2g_{(F)}$, $^3A_1g_{(F)} \rightarrow {}^3T_1g_{(p}$ $^3A_1g_{(F)} \rightarrow {}^3T_2g_{(F)}$
$[Cu(L_2)_2]Cl_2$	138	1.6	760, 383, 367, 344	13157.89, 26109.66 27247.95, 29069.76	$(^2E_{g\rightarrow} {}^2T_2g) =$ $^2B_1g \rightarrow {}^2A_1g$, $^2B_1g \rightarrow {}^2B_2g$ $^2B_1g \rightarrow {}^2E_1g$, CTLM
$[Zn(L_2)Cl_2]$	19	Dia	362, 263	27624.3, 38022.81	LMCT, Ligand (ILCT)
$[Zr(L_2)_2ClOH]Cl_2.3H_2O$	179	Dia	395, 360	25316.45, 27777.77	CT, Ligand (ILCT)

Dia: Diamagnetic.

3.5. The ^{1}H NMR and ^{13}C NMR spectra

The proposed ^{1}H and ^{13}C NMR chemical shifts of the Schiff base (ligand L2) are illustrated in **Figures 4-9** and **Table 4**.

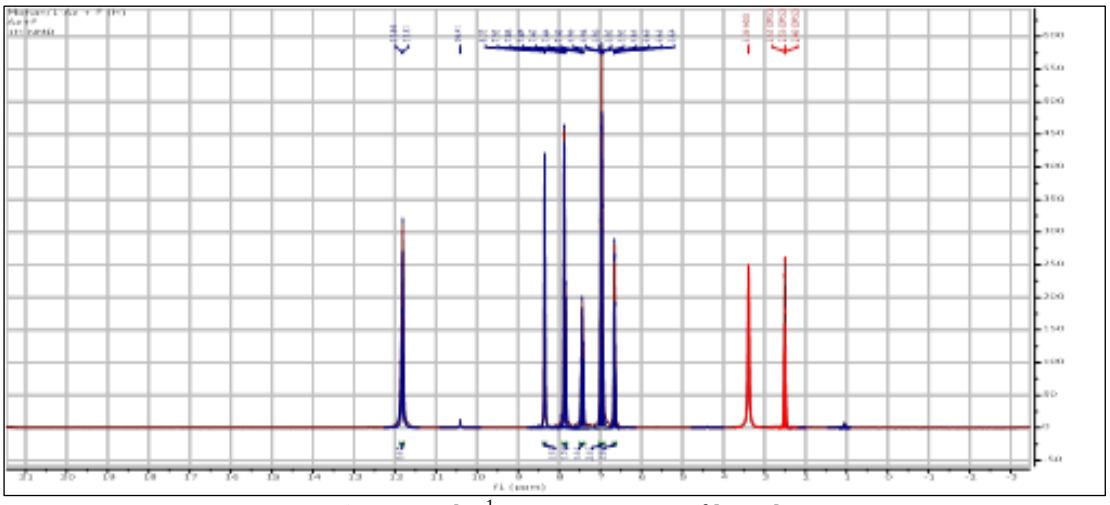

Figure 4. The ^{1}HNMR spectrum of ligand

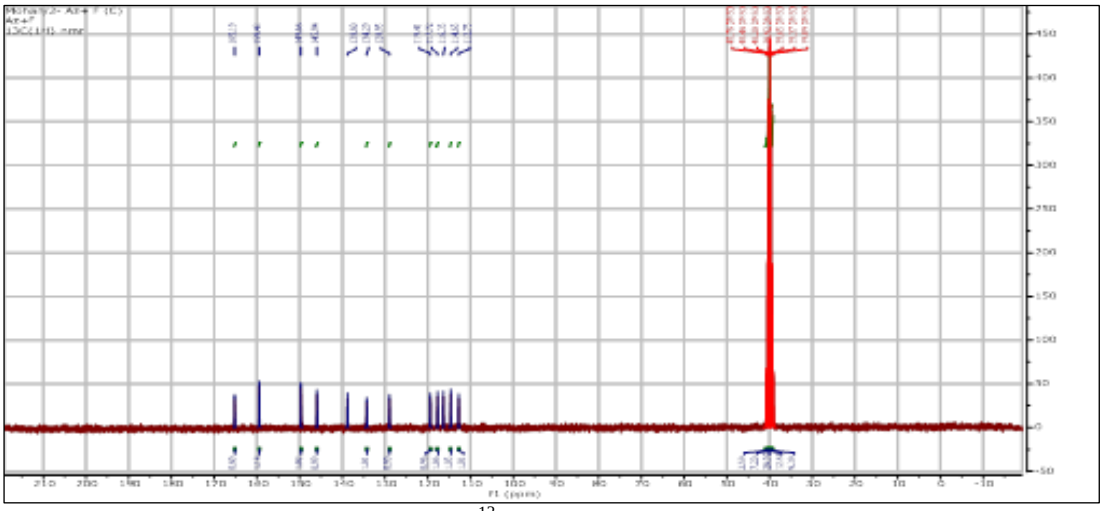

Figure 5. The ^{13}CNMR spectrum of ligand

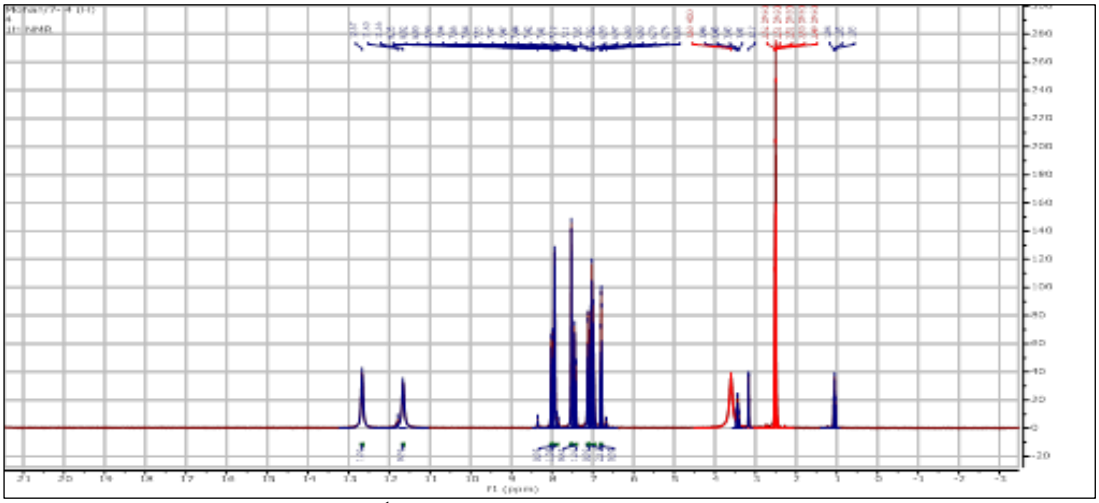

Figure 6. The ^{1}HNMR spectrum of [Zn $(L_2)_2Cl_2$] complexes

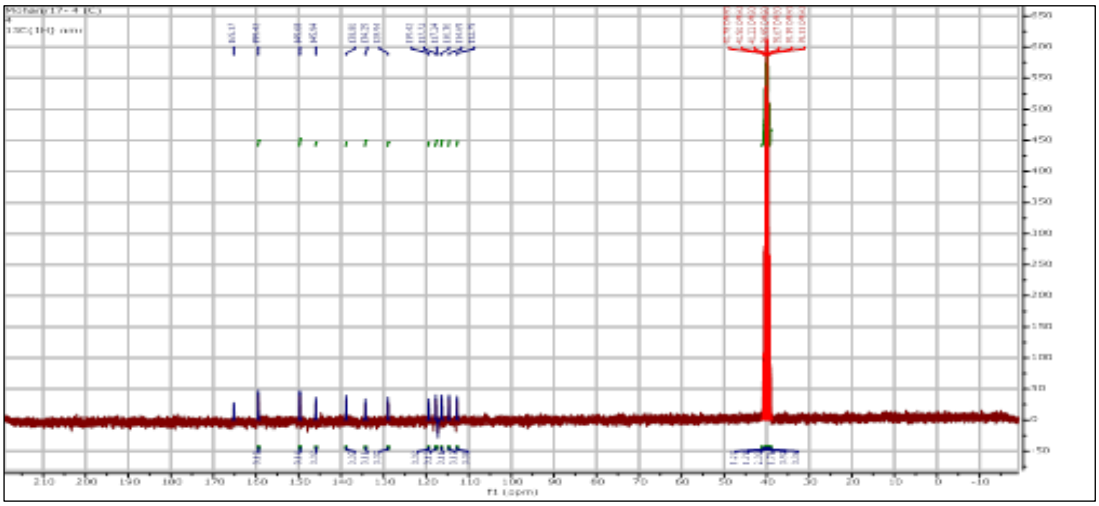

Figure 7. The ^{13}CNMR spectrum of $[Zn_2 (L_2)_2Cl_2]$ complexes

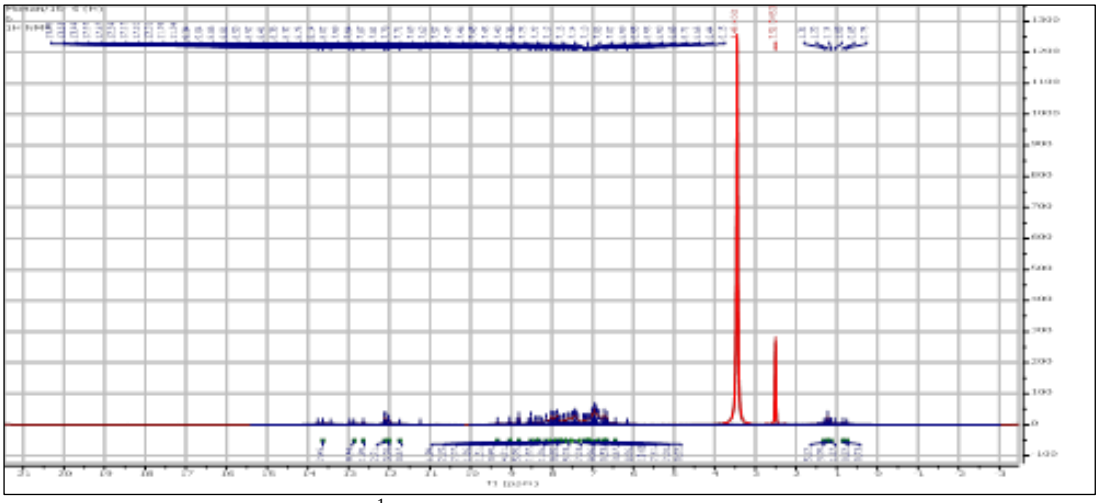

Figure 8. The ^{1}HNMR spectrum of $[Zr(L_2)_2ClOH]Cl_2 .3H_2O$

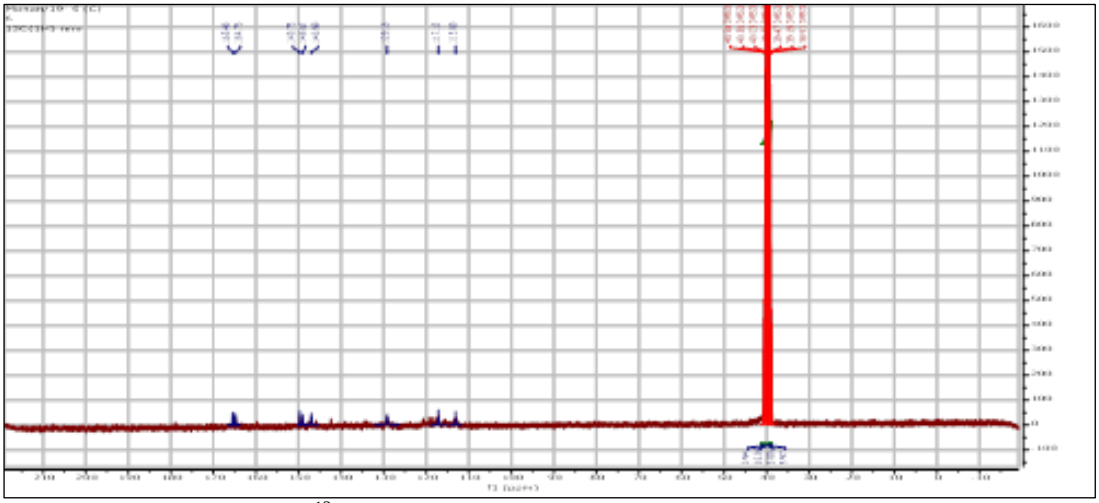

Figure 9. The ^{13}CNMR spectrum of $[Zr (L_2)_2ClOH]Cl_2.3H_2O$ complexes

Table 4. Proposed ^{1}H $^{13}CNMR$ chemical shifts (ppm) of schiff base (ligand L_2)

^{1}H NMR					
Compound	**DMSO**	**H-C**	**6H-C(Ar)**	**$1H^{+}$/NH**	**$1H^{+}$/OH**
Ligand	3.39(s),2.50(t)	3.5	6.65,6.96(q),7.44(t),7.48(d),8.35(s)	10.41	11.81(d)
ZnL_2	2.51,3.39	3.45	6.79,7.01,7.12,7.44,7.53,7.94,8.00	11.66	12.67
ZrL_2	2.5, 3.45	1.23, 1.05	6.71,6.85,6.96(dt),7.42(m),7.87, 7.98(m), 8.52, 8.81, 9.04, 9.34	11.74	13.63,12.64, 12.01, 12.11(d)
^{13}C NMR					
Compound	**DMSO**	**C- C**	**C = C**	**C- N**	**C = N**	**C = O**
L2 Ligand	39	119.41,117.72, 116.36,114.65,112.75	149.68,145.98,138.80,134.29	128.96	159.43	165.19
ZnL_2	39	119.42,117.72,117.24, 116.36,114.65, 112.75	149.68, 145.94, 138.80,134.29	128.94	159.24	165.17
ZrL_2	39.75	117.13, 113.09	149.73, 149.07, 146.07	129.16	164.76	165.46

3.6. Thermal analysis of TGA and DTG

The TGA/DTG analyses are shown in **Figures 10-12**, and the weight loss phases for the ligand and its complexes are demonstrated in **Table 5**.

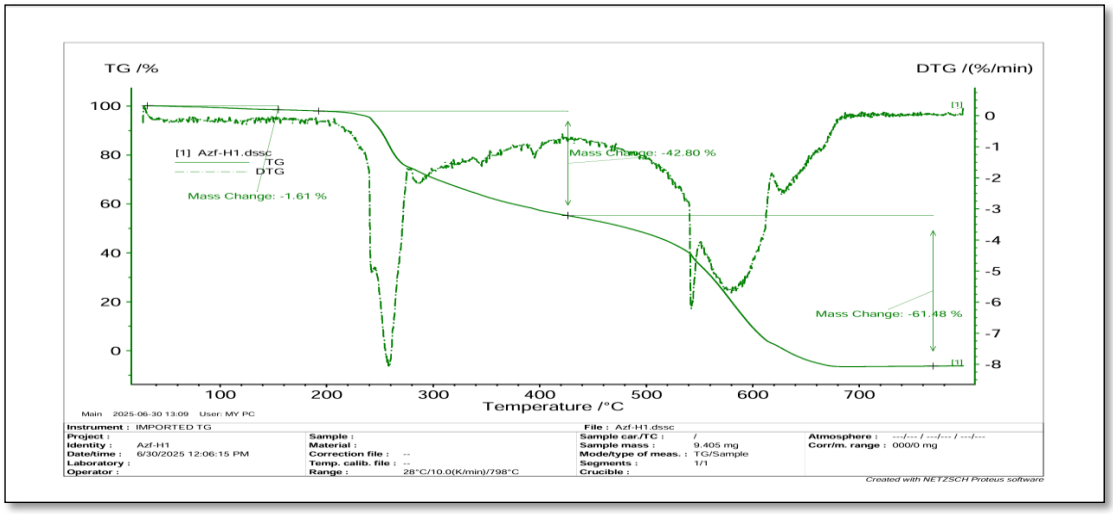

Figure 10. The TGA/DTG analysis of the Schiff base L_2

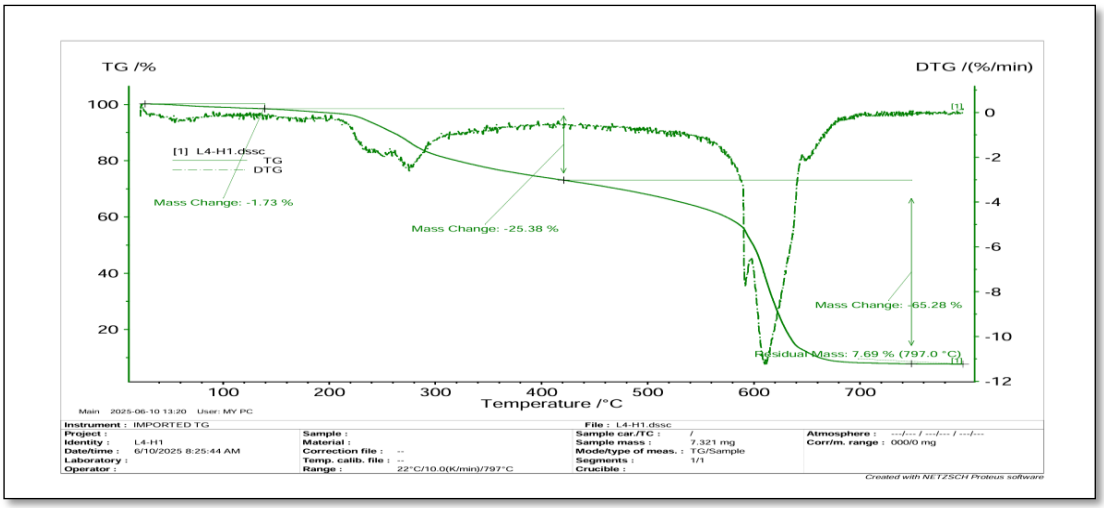

Figure 11. The TGA/DTG analysis of $[Zn\ (L)_2Cl_2]$

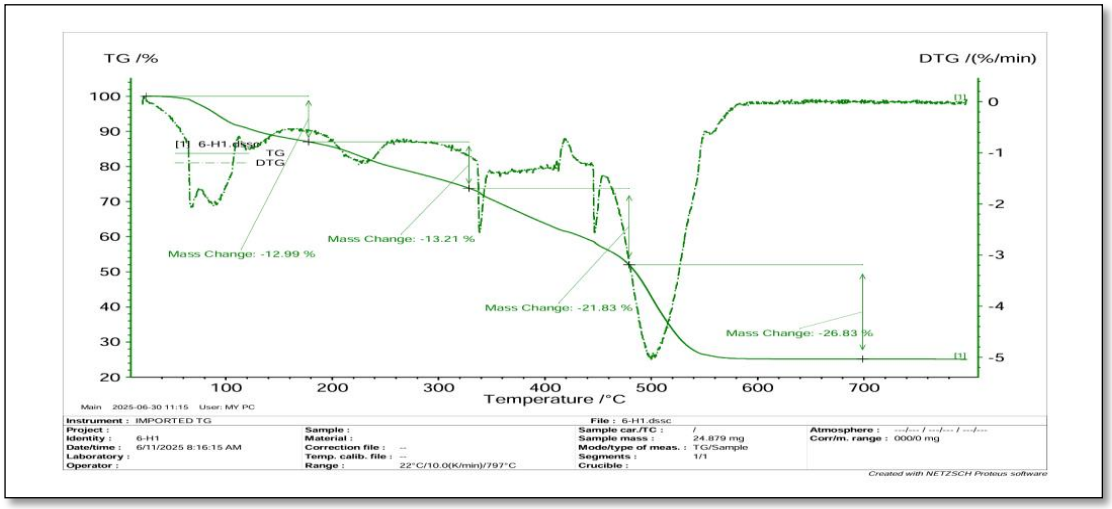

Figure 12. The TGA/DTG analysis of $[Zr\ (L)_2ClOH]Cl_2.3H_2O$ complex

Table 5. The weight loss phases for the ligand and its complexes

Formula	MWt g/mole	m/z	Fragment %	Average Temp. °C	Weight loss%			
					Cal.	Found	Product	Reaction
$C_{12}H_{10}N_2O_3$	230.1	230.9	I (-1.61)	80-150	-	3.704	Unknown	Endothermal
			II (-42.80)	150-420	94	98.48	C_5H_4NO	Exothermal
			III (-61.48)	420-770	136	141.465	$C_7H_6NO_2$	Endothermal
$C_{24}H_{19}N_4O_6ZnCl$	560	563,558	I (-1.73)	50-120	9.68	9.0998	-	Endothermal
			II (-25.38)	120-420	142	142.128	$C_5H_3N_2OCl$	Exothermal
			III (-65.28)	420-720	366	365.568	$C_{15}H_{12}N_2O_5Zn$	Endothermal
	Residue		=9.34	797	52	52.304	C_4H_4	
$C_{24}H_{27}N_4O_{10}ZrCl_3$	729		I (-12.99)	45-180	94	90.15	$Cl+2\ H_2O + NH_4$	Endothermal
			I (-13.21)	180-330	96	91.67	$Cl_2+ NH_6$	Exothermal
			III (-21.83)	330-480	159	159.14	C_9N_2O	Exothermal
			IV (-26.83)	480-700	195	195.59	$ZrC_{11}O_3H_6$	Endothermal
	Residue		25.14	.>600	182	183.27	ZrO_2+5C	----------

3.7. Inhibition of corrosion and biological activity

Zones of inhibition showing antifungal activities of Schiff base (L_2) and its complexes against isolated fungi are illustrated in **Table 6**.

Table 6. Zones (μm) of inhibition showing antibacterial activities of Schiff base (L_2) and its complexes against bacteria

Compound code	***Enterobacter faecalis* (ve+)**	***Streptococcus mutans* (ve+)**	***Pseudomonas aeruginosa* (ve-)**	***Staphylococcus aureus* (ve+)**	**Y2 *Bacillus***
Ligad L_2(1)	5	14	12	2	10
Ni-L_2(2)	4	12	13	1	7
Cu-L_2 (3)	6	15	13	2	8
Zr-L_2(4)	4	4	11	12	2
DMF	----	-----	----	-----	----
Chlorine 7%	----------	--------	--------	-------	15. 7
Chlorhexidine.*	3.69*	0.46*	------	------	
Kanamycin B**	-----	------	------	1.56**	------
CIP:Ciprofloxacin***	------	------	0.12***	0.12***	------
Nystatin****				N.A.	
Bacteria			**Fungi**		
Y2*(Bacillus)* 	under 100x oil-based magnification 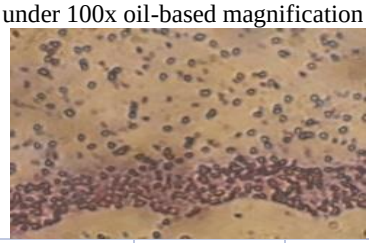		*Bortryis aclada* 	*Absidia carmbifera* 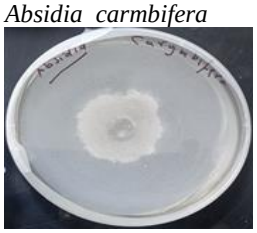	

Fungi	**L_2(1)**	**CuL_2(2)**	**Ni L_2(3)**	**ZnL_2(4)**	**CoL_2(5)**	**ZrL_2(7)**	**DMF**
Bortryis aclada	+	+	-	-	++	++	-
Absidiacarbifea	++	--	+-	---	+	--	-
Control							
fenhexamid	0.045% v/v against *bortryis fungi*[36]			Voriconazole	>16 against *Absidia fungi*[37]		

Control for Bacteria: Chlorhexidine*, Kanamycin B**, CIP: Ciprofloxacin.***, Nystatin.**** N.A = No activity[15-20] Y2: isolated pathogenic bacteria.

4. Discussion

4.1. Infrared spectroscopy

The observed vibrational patterns of the L_2 bond and its associated complexes exhibited a wide frequency range, indicating subsequent coordination changes with the metal. Most of these complexes showed a preference for ketohydrazone coordination over inohydrazone coordination with the metal. This preference is manifested in the carbonyl group maintaining its extension and density within a similar frequency range, while the extension of the NH bond persists in the 3200 cm^{-1} range, and the bond curvature remains within the (1500–1550)cm^{-1} range, despite metal-mediated coordination shifts. This coordination is associated with a decrease in electron density and a shift in the spectral peaks toward lower frequencies, where the functional groups retain their extensions, as described below. The result shows the FTIR spectra of the L_2 bond extensions and their metal complexes[21,22].

In {Mn, Ni, Co} complexes, the broad peak frequency of the OH group disappears, coinciding with the appearance of new peaks in the region between 400 and 600 cm^{-1} of the M-O bond. This indicates the compatibility of the hydroxyl (OH) group with the metal. Conductivity measurements and chlorine detection for the Ni complex showed negative results. In contrast, the Co-Mn complex produced a white precipitate with a conductivity consistent with that of a dichloroacetic electrolyte. This may indicate partial compatibility of the OH ions without proton removal, or it may be due to interference between the OH group and the hydrazide proton. The Co complex exhibited two peaks (3396 and 3375) cm^{-1}, suggesting either inconsistency or partial compatibility of the OH group. It also showed the formation of a white precipitate upon chlorine detection, with a conductivity of 137. The Zr complex exhibited broad peaks extending in the region between (3300-3400)cm^{-1}, representing extensions of the hydrazide proton and

inconsistent OH groups. Chlorine analysis yielded a white precipitate with conductivity, indicating the presence of inconsistent Cl ions.

4.2. Mass spectroscopy

The molar mass of the bond and its metallic components was determined using electron spray mass analysis (ESI-Mass). The bond spectrum showed a distinct peak with a mass-to-charge ratio (m/z) of 230.90, corresponding to a theoretically calculated molar mass of 231 g/mol. Similarly, the Zn compound mass spectrum showed a distinct peak for the bond, one of the compound's components, at m/z of 230.90. A peak also appeared at 526 g/mol, corresponding to the theoretically calculated molar mass of the Zn compound denoted by the formula $[Zn(L_2)_2]$. A series of peaks also appeared, which can be interpreted as 563 and 558 using the hypothetical formulas $[Zn(L_2)_2.2H^+]Cl$ and $[Zn(L)_2]^{+2}Cl$, respectively.

Several fragments were detected, indicating the mass of the Zr complex. A peak was observed at m/g = 230, which could represent the molar mass of the bond. Additionally, a peak at m/g = 372 ($LCl_3.2H_2O.4H^+$) and another at m/g = 462 could refer to $ZrLCl_3.2H_2O$. A third peak was observed at m/g = 558.75 ($Zr(L)_2+4H^+$). The absence of a peak in the compound may be attributed to its instability in the gaseous state. Compared to the bond, this is consistent with the fact that the bond is more stable than the compound in the gaseous state, as demonstrated by electron spray ionization analysis[23-25].

4.3. Electronic spectroscopy

Referring to result, the electronic spectra of the Schiff base and its metal complexes exhibited several electronic transitions. A distinct change in the appearance of transitions was observed in the visible region, specifically the d-d transitions of the metal complexes, which were not observed in the ligand region. This change suggests metal-like coordination of the ligand. The ligand spectrum showed three bands at 358, 276, and 238 nm, attributed to the ($\pi\rightarrow\pi^*$, $n\rightarrow\pi^*$, $n\rightarrow\pi^*$) transitions, respectively. The spectra of the Mn (II) complex showed several bands at 407, 363, and 340 nm, attributed to the ($^6A_1g \rightarrow {}^4T_1g$, $^6A_1g \rightarrow {}^4T_2g$, $\pi\rightarrow\pi^*$) transitions and CTLM transitions, respectively. The magnetic moment of the complex showed a value of (1.6) BM, which corresponds to hexagonal octahedral shapes. The Co compound also exhibited three new transitions in regions (674, 608, 361) nm, attributed to the transitions ($A_2g(F)\rightarrow T_1g(P)$, $A_2g(F)\rightarrow T_1g(F)$, $A_2g(F)\rightarrow T_2g(F)$). It also showed a value of (0.00) BM (the zero magnetic moment of the compound may indicate that Co (II) has oxidized to Co (III), possibly due to the carbonyl group possessing a strong electron-drawing force or that heat or exposure to air contributed to the metal's oxidation. This is consistent with octahedral hexagonal configurations. The Ni compound exhibited three transitions in the (990, 770, and 650) nm bands, attributed to the ($^3T_1g_{(F)}\rightarrow {}^3T_2g_{(F)}$, $^3T_1g_{(F)}\rightarrow {}^3T_1g_{(p)}$, and $^3T_1g_{(F)}\rightarrow {}^3T_2g_{(F)}$ transitions. The compound's properties were also observed, revealing a magnetic moment of 2.8 BM, consistent with a hexagonal octahedral structure. The Co compound exhibited several transitions in its spectrum, most notably at 760, 383, 367, and 344 nm, with a magnetic moment of 1.6 BM, corresponding to a single electron spin. These transitions are attributed to the ($^2B_1g\rightarrow {}^2A_1g$, $^2B_1g\rightarrow {}^2B_2g$, and $^2B_1g\rightarrow {}^2E_1g$) transitions, which appear as a single broad peak due to the Gann-Tiller effect, consistent with high-spin hexagonal shapes. In the Zn compound, the transitions were limited to 362, 263, and 233 nm, representing charge and bond transitions, respectively. No transitions were observed in the visible region due to the saturation of the d-shell, and a magnetic moment of less than one was present due to the lack of unpaired electrons. In the Zr compound, the spectrum showed transitions at 395 and 360 nm, attributed to (CT, ILCT) transitions, and a magnetic moment of less than one due to the absence of unpaired electrons, in the Zr ion shell[26]. It was observed that all compounds exhibited magnetic moments lower than the theoretical values. This is most likely due to a bonding property that lies between that of strong and weak bonds. This property results from a low electron density concentration on the metal and the sharing of pi orbitals in the bond, or perhaps from the formation of an antiferromagnetic coupling.

4.4. ^{1}H NMR and ^{13}C NMR spectra

Based on result, the compounds exhibit ^{1}H NMR shifts that differ significantly from those of the Schiff base. These shifts occur in all identified functional groups and in the aromatic ring protons. Furthermore, novel shifts appear that were not present in the Schiff base NMR spectrum. This strongly suggests metal conformation. The ^{13}C NMR spectrum of the compounds, documented in the same table, confirms a change in the bond spectrum through shifts in the carbon groups and the appearance of novel shifts not present in the bond spectrum or the Schiff base. This also suggests metal conformation[27-33].

4.5. Thermal analysis: TGA and DTG

The multiple weight loss stages in the thermogravimetric analysis demonstrated, first, the high stability of the prepared coordination compounds and the Schiff base. This is attributed to the chelating bond[34,35]. The reults illustrate the weight-loss stages, the proposed fractions of the lost mass, and the thermal process.

4.6. Inhibition of corrosion and biological activity

Schiff base solutions and their derivatives were prepared at a concentration of 0.001 M to evaluate their ability to inhibit the proliferation of biocorrosive isolates. The selected organisms included sulfur-reducing bacteria such as *Bacillus Y2*, as well as two fungal species, *Botrytis aclada* and *Absidia carbifera*. Additionally, 4 pathogenic bacteria were chosen for this study: Gram-positive bacteria, *Staphylococcus aureus*, and *Streptococcus mutans*, and *Enterococcus faecalis* and Gram-negative bacteria, *Pseudomonas aeruginosa*. The diffusion method was used in agar plates, and the diameter of the inhibition zone, was measured (mm). This selection aimed to evaluate the effects of the prepared samples and analyze the resistance levels of the biocorrosive isolates[36,37].

5. Conclusion

The multi-dentate Schiff base, denoted as L_2, was prepared using 2-hydroxybenzohydrazide and furfural, along with a range of its metal complexes in a 2:1 ratio. This resulted in a variety of octahedral complexes, some of which were electrolytic and some non-electrolytic. This variation in composition is attributed to the flexibility of the bond, which allows it to change position depending on the metal type and its oxidation state. Analyses using spectroscopic, analytical, and thermal methods, along with magnetic susceptibility and conductivity assessments, revealed the geometry of the L_2 metal Schiff base complexes. The molecular formulas of the complexes are as follows:

$[Mn(L_2)_2]Cl_2$,$[Co(L_2)_2]Cl_2$,$[Ni(L_2)_2]$,$[Cu(L_2)_2]Cl_2$,$[Zn(L_2)Cl_2]$,$[Zr(L_2)_2ClOH]Cl_2.3H_2O$.

The oxidation state of Co changed from $^{+}2$ to $^{+}3$ upon oxidation, and magnetic susceptibility measurements of the compound showed a magnetic moment of less than 1. The efficacy of these synthesized compounds was evaluated, and the results revealed varying levels of activity against specific bacterial isolates. Among them, the ligand showed the highest efficacy, while the compounds exhibited greater activity against pathogenic bacteria. Overall, resistance was observed in the isolates at a concentration of 10^{-3} M. This resistance appears to result from adaptation to harsh environments.

Acknowledgment

The authors extend their sincere thanks to the engineers and technicians at Al-Durra Refinery for their cooperation in collecting the study samples and providing their laboratory studies as a reference for us.

Conflict of Interest

The authors declare that they have no conflicts of interest.

Funding

No funding.

References

1. Little BJ, Lee JS. Microbiologically influenced corrosion. Hoboken (NJ): John Wiley & Sons; 2009. https://doi.org/10.1002/0471238961.micrlitt.a01.
2. Ali SI, Ahmad SN. Microbiologically influenced corrosion in uncoated and coated mild steel. Sci Rep. 2025; 15:12629. https://doi.org/10.1038/s41598-025-90003-5.
3. Li J, Chen L, Wei B, Xu J, Wei B, Sun C. Microbiologically influenced corrosion of circulating cooling systems in power plants– A review. Arab J Chem. 2024; 17(2):105529. https://doi.org/10.1016/j.arabjc.2023.105529.
4. Melo L. Biocorrosion of mild steel in drinking water conditions and disinfection. 1999.
5. Mohammed A, Ke Y, Afaque S, Ihsan Ul Haq T, Boxin W. Advances in microbial corrosion of metals induced via extracellular electron transfer by Shewanella oneidensis MR-1. npj Mater Degrad. 2025; 9(1): 1–15. https://doi.org/10.1038/s41529-025-00580-z.
6. Sastri VS. Types of corrosion inhibitor for managing corrosion in underground pipelines. In: Underground pipeline corrosion: detection, analysis and prevention. Cambridge: Woodhead Publishing; 2014; p. 166–211. https://doi.org/10.1533/9780857099266.1.166.
7. Czaban M. Aircraft corrosion – Review of corrosion processes and its effects in selected cases. Fatigue Aircr Struct. 2018; 10:5–20. https://doi.org/10.2478/fas-2018-0001.
8. Gerengi H, Kaya E, Solomon MM, Snape M, Koerdt A. Advances in the mitigation of microbiologically influenced concrete corrosion: A snapshot. Materials (Basel). 2024; 17(23):5846. https://doi.org/10.3390/ma17235846.
9. Ahmad N, Alam M, Wahab R, Ahmed M, Ahmad A. Synthesis, spectral and thermo-kinetics explorations of Schiff-base derived metal complexes. Open Chem. 2020; 18(1):1304–1315. https://doi.org/10.1515/chem-2020-0168.
10. Maiocchi A, Pedrini M, Ferrari V, Carreira ASA, D'Amore VM, Santoro F, Di Porzio A, Bosetti M, Cristofani R, Silvani A, Brancaccio D, Marinelli L, Di Leva FS, Provenzani A, Poletti A, Seneci P. Design, synthesis and characterization of aryl bis-guanyl hydrazones as RNA binders of C9orf72 G4C2 extended repeats. Eur J Med Chem. 2025; 293:117736. https://doi.org/10.1016/j.ejmech.2025.117736.
11. Saxena P, Samanta D, Gnimpieba EZ, Goh KM, Sani RK. Sulfate-reducing bacteria: Unraveling biofilm complexity, stress adaptation, and strategies for corrosion control. Sci Total Environ. 2025; 998: 180226. https://doi.org/10.1016/j.scitotenv.2025.180226.
12. Wang Y, Huang H, Tang Y, Wen S, Hou X. Influence of initial cell counts on the microbiologically influenced corrosion of L245N steel in shale gas environments. Bioelectrochemistry. 2026;168:109157. https://doi.org/10.1016/j.bioelechem.2025.109157.
13. Marzaq A, El Faydy M, Bazanov DR, Lozinskaya NA, Maatallah M, Kaichouh G, Allali M, Bazzi L, Dafali A, Zarrouk A. Effect of three substituted dihydroimidazole corrosion inhibitors on carbon steel surfaces: Experimental and theoretical studies of inhibition and adsorption performance. RSC Adv. 2025; 15(47):39807–39831. https://doi.org/10.1039/d5ra03853g.
14. Raczuk E, Dmochowska B, Samaszko-Fiertek J, Madaj J. Different Schiff bases—structure, importance and classification. Molecules. 2022; 27(3):787. https://doi.org/10.3390/molecules27030787.
15. Zhang F, Wen Q, Wang SF, Karim BS, Yang YS, Liu JJ, Zhu HL. Design, synthesis and antibacterial activities of 5-(pyrazin-2-yl)-4H-1,2,4-triazole-3-thiol derivatives containing Schiff base formation as FabH inhibitory. Bioorg Med Chem Lett. 2014; 24(1):90–95. https://doi.org/10.1016/j.bmcl.2013.11.079.
16. Sampiron EG, Costacurta GF, Baldin VP, Almeida AL, Ieque AL, Santos NC, Alves-Olher VG, Vandresen F, Gimenes AC, Siqueira VL, Caleffi-Ferracioli KR, Cardoso RF, Scodro RB. Hydrazone, benzohydrazones and isoniazid-acylhydrazones as potential antituberculosis agents. Future Microbiol. 2019; 14(11):981–994. https://doi.org/10.2217/fmb-2019-0040.
17. Omidi S, Kakanejadifard A. A review on biological activities of Schiff base, hydrazone, and oxime derivatives of curcumin. RSC Adv. 2020; 10(50):30186–30202. https://doi.org/10.1039/d0ra05720g.

18. Chau AS, Chen G, McNicholas PM, Mann PA. Molecular basis for enhanced activity of posaconazole against *Absidia corymbifera* and *Rhizopus oryzae*. Antimicrob Agents Chemother. 2006; 50(11): 3917-3919. https://doi.org/10.1128/aac.00747-06.
19. Carreño A, Páez-Hernández D, Cantero-López P, Zúñiga C, Nevermann J, Ramírez-Osorio A, Gacitúa M, Oyarzún P, Sáez-Cortez F, Polanco R, Otero C, Fuentes JAA. Structural characterization, DFT calculation, NCI, scan-rate analysis and antifungal activity against *Botrytis cinerea* of (E)-2-{[(2-aminopyridin-2-yl)imino]-methyl-4,6-di-tert-butylphenol (pyridine Schiff base). Molecules. 2020; 25(12): 2741. https://doi.org/10.3390/molecules25122741.
20. Rupa SA, Moni MR, Patwary MAM, Mahmud MM, Haque MA, Uddin J, Abedin SMT. Synthesis of novel tritopic hydrazone ligands: Spectroscopy, biological activity, DFT, and molecular docking studies. Molecules. 2022; 27(5):1656. https://doi.org/10.3390/molecules27051656.
21. Bhaskar RS, Ladole CA, Salunkhe NG, Aswar AS. Synthesis, characterization and biological studies of some transition metal complexes with pyrazine Schiff base hydrazone ligand. Jordan J Chem. 2020; 15(2):61–72. https://doi.org/10.47014/15.2.2.
22. Pospieszna-Markiewicz I, Fik-Jaskółka MA, Hnatejko Z, Patroniak V, Kubicki M. Synthesis and characterization of lanthanide metal ion complexes of new polydentate hydrazone Schiff base ligand. Molecules. 2022; 27(23):8390. https://doi.org/10.3390/molecules27238390.
23. Husseini M, Latief BH, Khudhair NA, Huseeni MD, Al-Saadi FA. Investigation of corrosion inhibition of carbon steel by using natural Iraqi plum tree gum in a saline medium. Iraqi J Sci. 2024; 65(10):5349-5356. https://doi.org/10.24996/ijs.2024.65.10.1.
24. Munir R, Javid N, Zia-ur-Rehman M, Zaheer M, Huma R, Roohi A, Athar MM. Synthesis of novel N-acylhydrazones and their C–N/N–N bond conformational characterization by NMR spectroscopy. Molecules. 2021; 26(16):4908. https://doi.org/10.3390/molecules26164908.
25. Preethi V, Vijukumar VG, Anila Raj S, Vidya VG. Synthesis, characterization, DFT studies and evaluation of the potential anti-tumour activity of nicotinic hydrazide based Schiff base using in vitro and molecular docking techniques. Heliyon. 2024; 10(9):e29689. https://doi.org/10.1016/j.heliyon.2024.e29689.
26. Zhongying X, Xuewen C, Yefei W, Michal S, Stanislav U, Shanjian L, Ying T. Effective corrosion inhibitor of mild steel in marine environments: Synthesis and application of hydrazides. Sustain Mater Technol. 2023; 38:e00747. https://doi.org/10.1016/j.susmat.2023.e00747.
27. Markert C, Thinius M, Lehmann L, Heintz C, Stappert F, Wissdorf W, Kersten H, Benter T, Schneider BB, Covey TR. Observation of charged droplets from electrospray ionization plumes in API mass spectrometers. Anal Bioanal Chem. 2021; 413(22):5587-5600. https://doi.org/10.1007/s00216-021-03452-y.
28. Shi ZQ, Ji NN, Hu HL. One-pot concomitant preparation of two copper(II) coordination polymers with different configurations of bridging bithiophene ligands. Acta Cryst C Struct Chem. 2020; 76(Pt 1):37–43. https://doi.org/10.1107/S2053229619016024.
29. Al-Hakimi AN, Alminderej F, Aroua L, Alhag SK, Alfaifi MY, Mahyoub JA, Alnafisah AS. Design, synthesis, characterization of zirconium(IV), cadmium(II) and iron(III) complexes derived from Schiff base 2-aminomethylbenzimidazole, 2-hydroxynaphtadehyde and evaluation of their biological activity. Arab J Chem. 2020; 13(10):7378–7389. https://doi.org/10.1016/j.arabjc.2020.08.014.
30. Hijazi AK, Taha ZA, Issa DK, Alshare HM, Al-Momani WM, Elrashidi A, Barham AS. Synthesis, characterization and catalytic/antimicrobial activities of some transition metal complexes derived from benzohydrazide Schiff base. Molecules. 2024; 29(23):5758. https://doi.org/10.3390/molecules29235758.
31. Komyha EM, Mahmoud WH, Hosny WM, El-Sherif AA. Design, structural characterization, molecular docking and biomedical applications of hydrazone-based Schiff base metal complexes. Egypt J Chem. 2023; 66(13):1219–1230. https://doi.org/10.21608/ejchem.2023.147796.6650.
32. Kostova I, Manolov I, Karaivanova M. Synthesis, physicochemical characterization, and cytotoxic screening of new zirconium complexes with coumarin derivatives. Arch Pharm (Weinheim). 2001; 334(5):157-162. https://doi.org/10.1002/15214184(200105)334:5<157::AIDARDP157>3.0.CO;2-S.
33. Yadav P, Sarkar A, Singh A, Singh AK, Nirala RK, Naqvi I, Verma D, Jit BP, Jaiswal M, Rath R. Spectral characterization and biological activities of hydrazide Schiff base metal complexes. Corros Prot. 2023; 51(2):832–849.

34. Senila L, Hoaghia A, Moldovan A, Török IA, Kovacs D, Simedru D, Senila M. The potential application of natural clinoptilolite-rich zeolite as support for bacterial community formation for wastewater treatment. Materials (Basel). 2022; 15(10):3685. https://doi.org/10.3390/ma15103685.
35. Jabeen M. A comprehensive review on analytical applications of hydrazone derivatives. J Turk Chem Soc A Chem. 2022; 9(3):663–698. https://doi.org/10.18596/jotcsa.1020357 .
36. Shi X, Zhang R, Sand W, Mathivanan K, Zhang Y, Wang N, Duan J, Hou B. Comprehensive review on the use of biocides in microbiologically influenced corrosion. Microorganisms. 2023; 11(9):2194. https://doi.org/10.3390/microorganisms11092194.
37. Giriraju A, Yunus GY. Assessment of antimicrobial potential of 10% ginger extract against *Streptococcus mutans*, *Candida albicans*, and *Enterococcus faecalis*: An in vitro study. Indian J Dent Res. 2013; 24(4):397–400. https://doi.org/10.4103/0970-9290.118356.